Ahmed, Tamer M.
Elaghbash, Ahmed O.
Banawan, Adel A.
Ahmed, Yasser M.
Hassan, Amany M.

NUMERICAL PREDICTION OF SOLITARY WAVE FORMATION OF A PLANING HULL IN SHALLOW WATER CHANNELS

Summary

This paper uses a CFD (Computational Fluid Dynamics) analysis to investigate the shallow water effects on prismatic planing hull. The turbulence flow around the hull was described by Reynolds Navier Stokes equations RANSE using the k-ε turbulence model. The free surface was modelled by the volume of fluid (VOF) method. The analysis was steady for all the range of speeds except those close to the critical speed range due to the propagation of the planing hull solitary waves at this range. In this study, the planing hull lift force, total resistance, and wave pattern for the range of subcritical speeds, critical speeds, and supercritical speeds have been calculated using CFD. The numerical results have been compared with experimental results. The pressure distribution on the planing hull and its wave pattern at critical speed in shallow water were compared with those in deep water.

Keywords: *Shallow channel; CFD; planing hull; deep water; solitary wave; numerical investigation; critical speed; wave pattern; open water*

Nomenclature

L   length of planing hull (m)
b   beam (m)
H   depth of water (m)
V   speed of model (m/s)
g   gravitational acceleration (m/s2)
R_T total resistance (N)
L_F lift force (N)
C_v beam Froude number, $\mathbf{Cv} = V/\sqrt{g*b}$

F_h water depth Froude number $F_h = V/\sqrt{g*H}$
ν   Kinematic viscosity (m2/s)
P Pressure (N/m2)
ρ Density of fluid (kg/m3)
Lc   chine wetted length (m)
N   normal force (N)

1. Introduction

Recently, the simulation of the hydrodynamic performance of planing hull sailing in shallow water has become a common practice in the yachts building community. Hence, it is more used for the high-speed boats which sailing near to shoreline compared with where yachts

used to navigate before [1]. The high demand for high-speed boats operating near shore requires good knowledge of its behaviour in three regions of speed, (subcritical, critical, and supercritical). Various methods are available for calculating hydrodynamic characteristics of planing hull such as; analytical, numerical, and, experimental methods. Experimental methods require expensive facilities and measurement tools to be conducted. This significantly increases the cost and time –required to obtain results- as compared to numerical methods. There has been a surge in the use of numerical methods for investigating the resistance of small boats and ships in different waterways whether it be, shallow channels or open water.

The first theoretical formula to consider the calculation of maximum pressure around planing 2D sections was proposed by Kerman [2]. His work remained in use until equations for 3D planing surfaces by Savander and Scorpio [3] were introduced.

The finite difference method was used to solve the Kadomtsev-Petviashvili equation for a ship moving near critical speed [4] to estimate the; moment, lift force, wave pattern, solitary wave and, wave resistance. Many experiments were conducted in an attempt to calculate the force and the moment on the flat bottom hull in shallow water at fixed trim by Christopher [5]. Furthermore, the force and moment on a constant deadrise angle prismatic hull by Reyling [6] were obtained experimentally.

For series 62 hull form, residuary resistance was computed over a range of speeds from displacement speeds to planing speeds when the hull moving in shallow water and it was concluded that there is an increase in residual resistance at the subcritical speed range and a decrease at the supercritical speed range as compared to deep water. Besides, there was a resistance hump created at the maximum angle of trim and the highest value of sinkage.

The 2D+t potential flow method was used to investigate the performance of planing hulls in calm water and was compared with 3D Reynolds Navier Stokes Equation (RANSE) method by Iafrati and Broglia [7]. These methods found the optimal drag and dynamic stability for the stepped planing hull [8]. The validation of the 2D+t model for single stepped planing hull with the experimental data in terms of; resistance, dynamic trim, and wetted surface area was carried out by Bilandi [9]

The RANSE method was used to predict moment and force on a planing prismatic hull with a constant deadrise angle equal to 20 degrees by Brizzolara and Serra [10]. Safari calculated; total resistance, added resistance, and wave pattern numerically [11]. Mancini used this analysis to get; total resistance coefficients, wetted surfaces, and dynamic trim for warped planing hull [12]. Moreover, heave motion, pitch angle, free surface deformation, and resistance of planing vessels were obtained through this analysis by Wang [13] in deep water. Also, the modern transverse stepped planing hull was investigated by CFD, which applies moving mesh techniques and large eddy simulation to find the total resistance, trim, and sinkage. These numerical results were validated with experimental results [14]. Moreover, Bakhtiari estimated; the numerical results of drag, pressure distribution, wetted surface, water spray, and wave generation by stepped planing hull [15]. Furthermore, the wake profile was compared by Savitsky and Morabito empirical formula. The morphing mesh method and k-ε model were used to simulate the fluid flow around the two-stepped hull moving freely to heave and pitch [16]. Also, this mesh technique was used to describe hydrodynamic characteristics around the tunneled planing hull and it's compared with experimental results [17].

The Smoothed Particle Hydrodynamics method investigated the pressure distribution on the seafloor in very shallow water and, the change in the angle of created divergent waves over a range of speeds [1].

The work presented here within sheds light on the hydrodynamics of a prismatic planing flat bottom hull operating in a shallow water channel as compared to its hydrodynamics in open water; taking into account the transition from displacement speeds to planning speeds. At

planing speeds, the hull is supported by both, buoyancy and lift forces which puts the hull in position. Wave making resistance is the main component of the total resistance. The generated waves system includes transverse and divergent waves. Divergent waves make an angle of 19.47 degrees at subcritical speeds (Kelvin wave pattern) and 90 degrees at critical speeds. This angle decreases at supercritical speeds.

2. Overview of experimental data

The model employed in this study is similar to the one used in the experiments conducted by Demarco et.al [14] on the model hull shown in Figure 1. The model is box-shaped whose dimensions are (length 914mm, beam 183mm, depth 102mm) with a circumferential groove (9mm high × 6mm deep) around the model. The groove is located 9mm above the bottom.
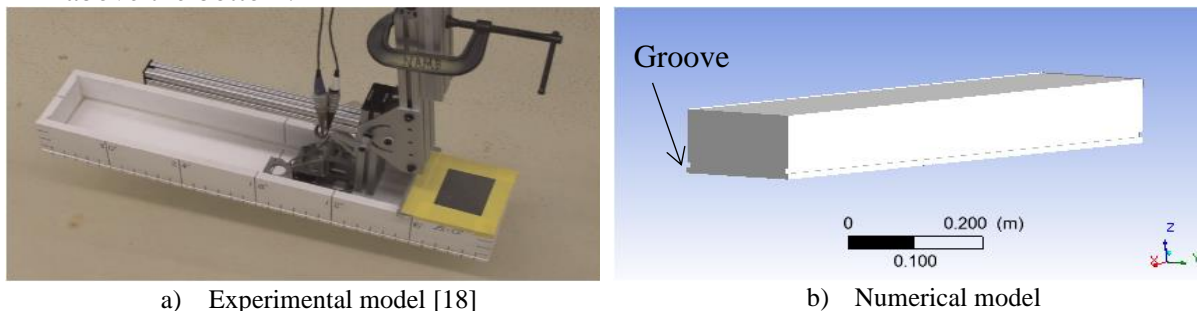
| a) Experimental model [18] | b) Numerical model |

Figure 1 Planing hull model a) Experimental model (Morabito, 2013) b) Numerical model.

The test was adopted by moving the model through the channel at a constant sinkage and trim by aft is equal to 6 degrees. The hull model is examined in calm water at a range of speed from 0.3 m/s to 3.7 m/s for water depths 0.5b, 0.75b, 3b, 8b.

The objectives of Morabito experimental measurement were the tangential force and normal force on the bottom of the hull separately using a dynamometer, also some measurements were calculated as the change on wetted chine length (L_C), and transom ventilation (Y_K) at all a range of speed. For that, the hull is divided into suctions and water lines shown in Figure 1 a.

3. Computational and analysis methods

In this work, the finite volume RANS code (ANSYS CFX) is used to study the flow about a small planing hull craft operating in a shallow channel at water depth 0.5b to predict the hydrodynamic forces (acting on) and wave patterns (generated by the hull) at subcritical, critical and supercritical speeds.

In this investigation, the k-ε turbulence model is adopted guided by previous work [9]. In the critical speed region and when the ship velocity is equal to the velocity of the generated wave in the shallow channel, a solitary wave starts to generate. The solitary waveform is of a wave single crest and moves forward through the channel. A transient analysis is required at the critical speed as shown in Table 1. The analysis at subcritical and supercritical speeds is steady as shown in Table 2.

Table 1 analysis setting at critical speeds

analysis type	transient
number of element	6000000
Total time	25 sec
turbulent model	k-ε
time step	0.2 sec

Table 2 analysis setting at subcritical and supercritical speeds

analysis type	Steady-state
number of element	6000000
Residual	e^-5
Max iteration	10000
turbulent model	k-ε

3.1 Mathematical model

The flow about the model is assumed to be incompressible turbulent flow. Hence, the governing equations are the continuity and momentum equations given as follows.

$$\frac{\partial u}{\partial x} + \frac{\partial v}{\partial y} + \frac{\partial w}{\partial z} = 0 \tag{1}$$

$$\frac{\partial \overline{U_i}}{\partial t} + \overline{U_j}\frac{\partial \overline{U_i}}{\partial x_j} = -\frac{1}{\rho}\frac{\partial \overline{P}}{\partial x_i} + \nu\frac{\partial^2 \overline{U_i}}{\partial x_j \partial x_j} - \frac{\partial \overline{u_i u_j}}{\partial x_j} + g_i \tag{2}$$

The Reynolds stress tensor $\overline{u_i u_j}$ represents the change of momentum cross the free-surface which occurs as result for surface tension force, the color function describes the free-surface as the volume of fraction γ

$$\frac{\partial \gamma}{\partial t} + U_i\frac{\partial \gamma}{\partial x_i} = 0 \tag{3}$$

Based on the volume of fluid (VOF) method, the air-water interface is described implicitly. The volume of fraction γ represents the percentage of water at each cell at the free surface to describe the interference between the two fluids. The magnitude of γ for each cell cut by the free surface is between 0 and 1 ($0 < \gamma < 1$). While the volume fraction γ equals 1 for total water occupancy, it equals 0 for total air

$$\rho_{ij} = \gamma_{ij}\rho_w + (1 - \gamma_{ij})\rho_a \tag{4}$$

$$\mu_{ij} = \gamma_{ij}\mu_w + (1 - \gamma_{ij})\mu_a \tag{5}$$

Where ρ and μ at any cell (denoted by ij) can be computed using γ by taking a simple volume average over the cell. In addition, (a) and (w) refer to air and water, respectively.

When the Froude depth equals 1, the speed of the ship equals the speed of the wave (V) and can be calculated by

$$V = \sqrt{g * H} \tag{6}$$

3.2 Numerical domain and Boundary conditions

Due to the symmetry of the hull, only half of the computational domain is represented in the CFD simulations of this study with dimensions shown in Figure 2. The hull is implemented with a fixed trim of 6 degrees and fixed heave giving a transom draft of 0.05673m, such as that in the experimental work. The study is carried out to simulate a shallow channel whose water depth is 0.1L and width is 1.3L. The reference point of the computational domain is at G= (0, 0, 0). Boundary conditions imposed on the numerical domain are shown in Table 3. The air-water flows through the shallow channel from inlet to outlet about the hull. These investigations cover a range of speeds from 0.3 m/s to 3.7 m/s. This range includes the three regions of the subcritical, critical, and supercritical speeds. Also, when the analysis for deep water, the high seabed equal to 2.46L. This height ensures no effect for seabed on the hull resistance.

In the current study, the wall bounding effects are very important and have a significant effect on the hull form drag at different speeds. Figure 3 shows the distribution y$^+$ on the hull which the value around 30 to 300.
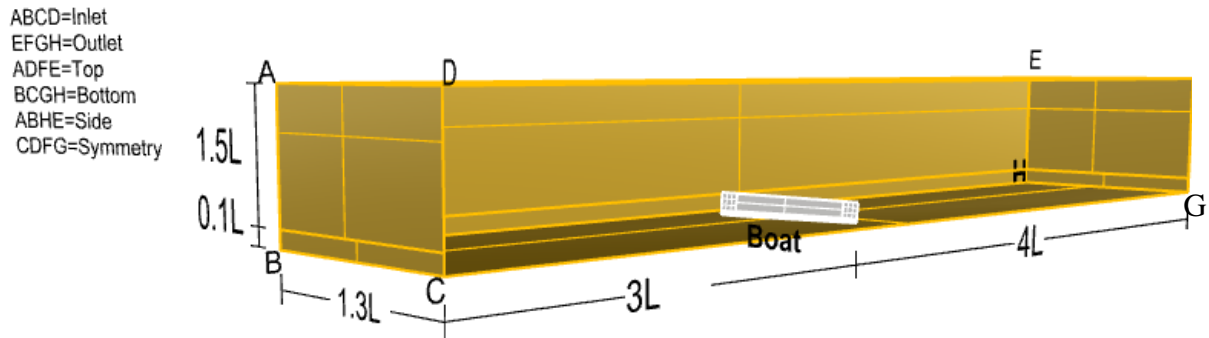
Numerical prediction of solitary wave formation for
Planing hull in shallow water channels

Tamer M. Ahmed, Ahmed O. Elaghbash,
Adel A. Banawan, Yasser M. Ahmed, Amany M. Hassan.

Figure 2 Dimension and boundary conditions of the numerical domain

a) hull side b) hull bottom
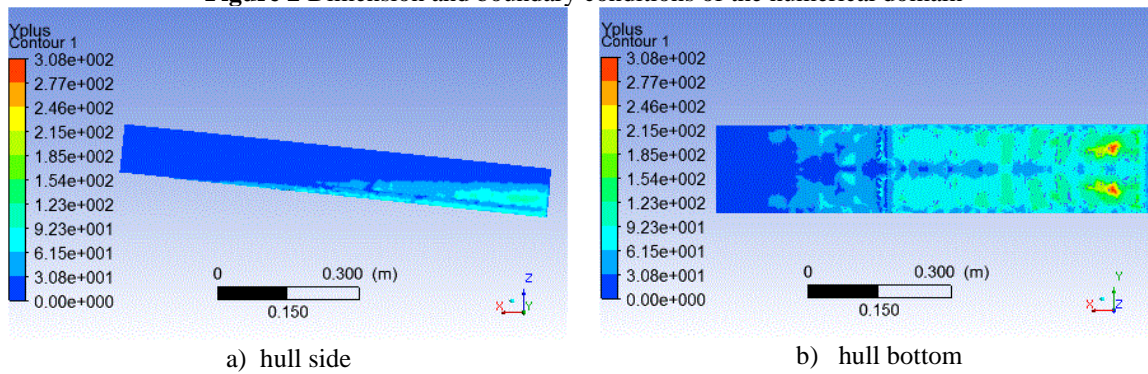
Figure 3 distribution y^+ on the hull

Table 3 boundary conditions details

Position	type	boundary condition
Boat	No-slip	wall
Inlet	velocity	inlet
Outlet	static pressure	outlet
Top	free slip	wall
Side	free slip	wall
Bottom	free slip	wall
Symmetry	-	symmetry

3.3 Mesh generation strategy

Code ICEM CFD is used to generate an unstructured mesh grid required for the CFD code solver. The number of mesh elements generated -in one domain- and shown in Figure 4 equals 6 million elements. Accuracy of results is dependent on the quality of the mesh grid which is affected by the element size, type, and algorithm. The number of mesh elements is increased over the planing hull surface and its vicinity to improve the accuracy of numerical predictions of resistance and wave patterns generated at different forward speeds. The mesh density function is applied at the free-surface region throughout the whole computational domain to better predict the generated wave patterns by the hull. A refined mesh is generated at the bottom of the computational domain to accurately predict the effect of the channel bottom on the hull resistance.
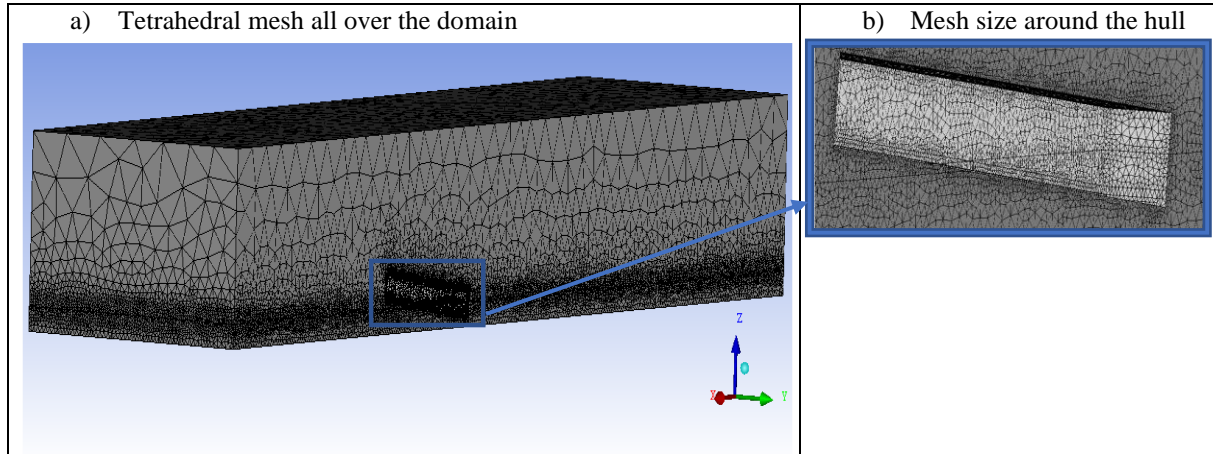
a)   Tetrahedral mesh all over the domain   b)   Mesh size around the hull

Figure 4 Schematic illustration of generated mesh in the domain. a) Tetrahedral mesh all over the domain b) Mesh size around the hull

4. Results and discussion

This study predicted total resistance, generated wave pattern and, lift force of a planing hull model moving in a shallow channel over three regions of speed, (subcritical, critical, and supercritical). Numerical results were validated by comparison with experimental data available in the literature [14].

4.1 Comparison of numerical and experimental results

This part of the paper is compared available experimental results; wetted length, dynamic normal force over displacement, and lift force coefficient with the numerical results. Notice that, at the critical speed range the value of results fluctuates. For that, the mean value obtained numerically and compared with the mean value experimentally. The mean value of results can be calculated as

$$Xm = \frac{\sum_{k=1}^{k=n} X_k}{n} \tag{7}$$

Where
X_m = mean result at a critical speed
n = number of results
X_k = results at a critical speed.

4.1.1   Wetted length L_c

The wetted length expresses the chine length under the waterline. Figure 5 shows the comparison between the wetted length to beam ratio of the model versus Froude depth numerically and experimentally. When the Froude depth near to 1, the wetted length increases, as a result of solitary wave formation at the critical speeds range. However, all the range of numerical results achieved an error of around 4.8 % compared with experimental results. The maximum error at F_h= 1.27 is equal to 31.3 %. Approximately, at the supercritical speeds range, the wetted length is steady at 3.45 while, at subcritical speeds, it's slightly fluctuated around 3.25. In general, the numerical results of L_c/b showed an excellent agreement with the results of the experiment.
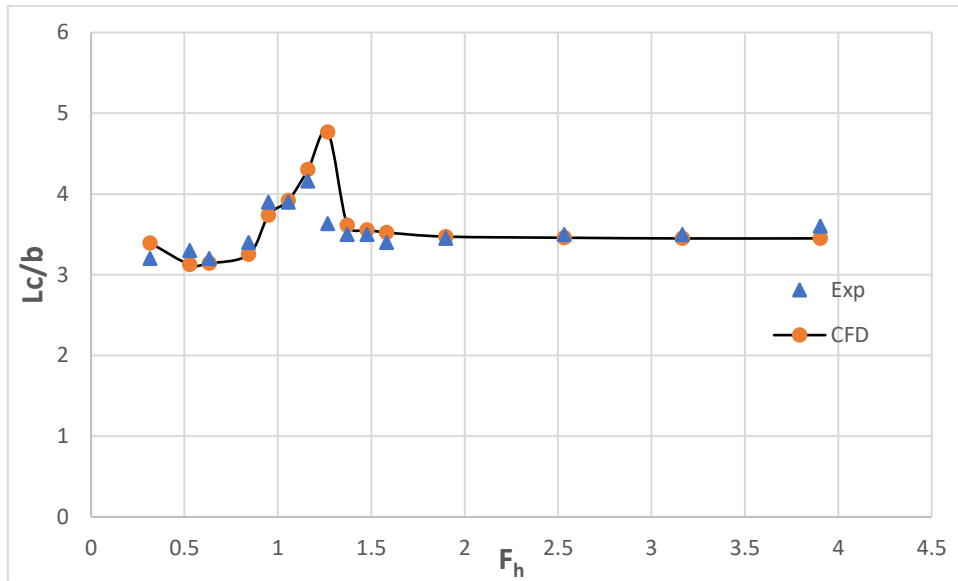
Numerical prediction of solitary wave formation for
Planing hull in shallow water channels

Tamer M. Ahmed, Ahmed O. Elaghbash,
Adel A. Banawan, Yasser M. Ahmed, Amany M. Hassan.

Figure 5 Comparison between experimental and CFD results of wetted length/beam ratio at different Froude depth

5.1.2 Normal force (N)

The normal force means the hydrodynamic force acts perpendicularly to the hull bottom. Figure 6 shows the dynamic normal force to static buoyancy force ratio, versus the Froude beam (C_V) numerically and experimentally. The experimental normal force ratio slightly decreases below zero at low speeds range before fully ventilation at the transom occurs, it means the dynamic force applies suction on the hull toward the channel bed (squat force). The numerical normal force slightly decreases at partial ventilation. Then increases rapidly until the dynamic force equal to displacement force at full ventilation at transom as result for hydrodynamic lift, at this range the largest deviation between experimental and numerical results occurs. After that, the curve increases sharply without a considerable deviation between numerical and experimental results. The numerical results are lined with experimental results.
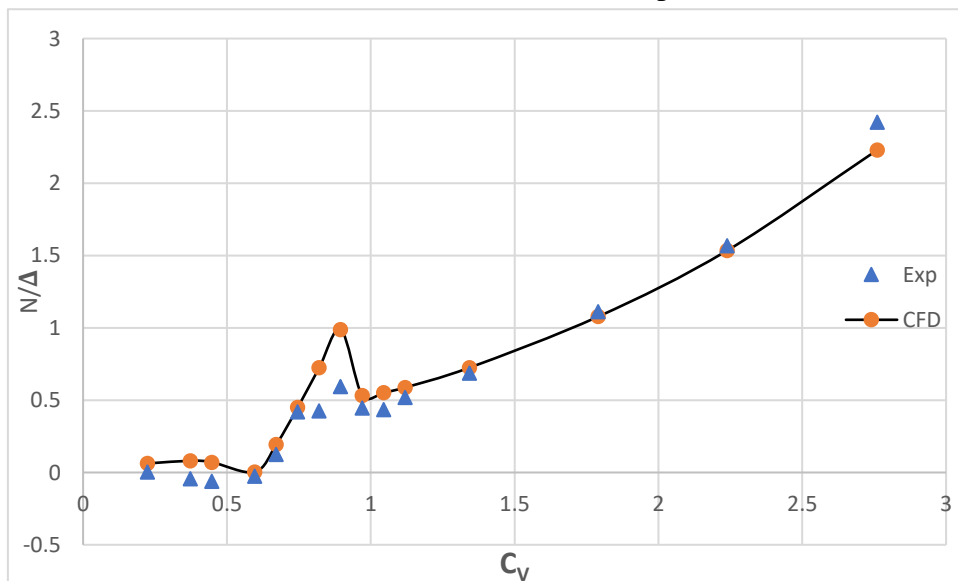
Figure 6 dynamic normal force/static normal force ratio N/Δ versus C_v numerically and experimentally

5.1.3 Total resistance R_T

A comparison between the numerical total resistance and experimental total resistance is shown in Figure 7. The two curves increase sharply over the critical Froude number's range

(F_h=0.84 to F_h=1.27). After that, there is a slight drop in values and then they increase gradually over the supercritical Froude number's range (F_h=1.37 to F_h=3.9). Very good agreement between the two curves is observed over –almost- the whole range of Froude numbers albeit, the error increases at Froude number close to the peak. The total average error between the numerical and experimental total resistance is no more than 8%. The maximum error is observed at the maximum critical Froude-depth number of 1.27 and is equal to 26%.
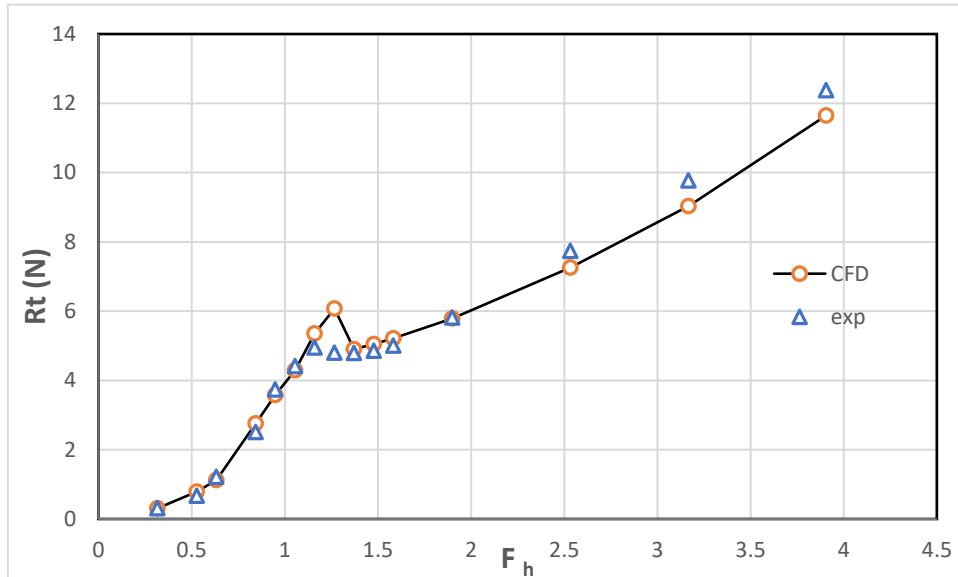

Figure 7 Experimental and numerical total resistance

5.1.4 Hydrodynamic Lift Force L_F

A comparison between the numerical and experimental total lift force is shown in Figure 8. In general, the lift force decreases slightly over the supercritical range (from F_h=0.32 to F_h=0.63). There is a numerical over prediction of the lift force in this range. However, the lift force increases rapidly over the critical speed range (from F_h=0.84 to F_h=1.27). Subsequently, the value of the lift force rises gradually over the supercritical range. The total average error equals to 7%, while the maximum error is 34% at the maximum critical Froude-depth number. For the whole range of speeds, very good agreement is observed between the numerical and experimental lift force except the maximum critical speed of 1.2m/s.
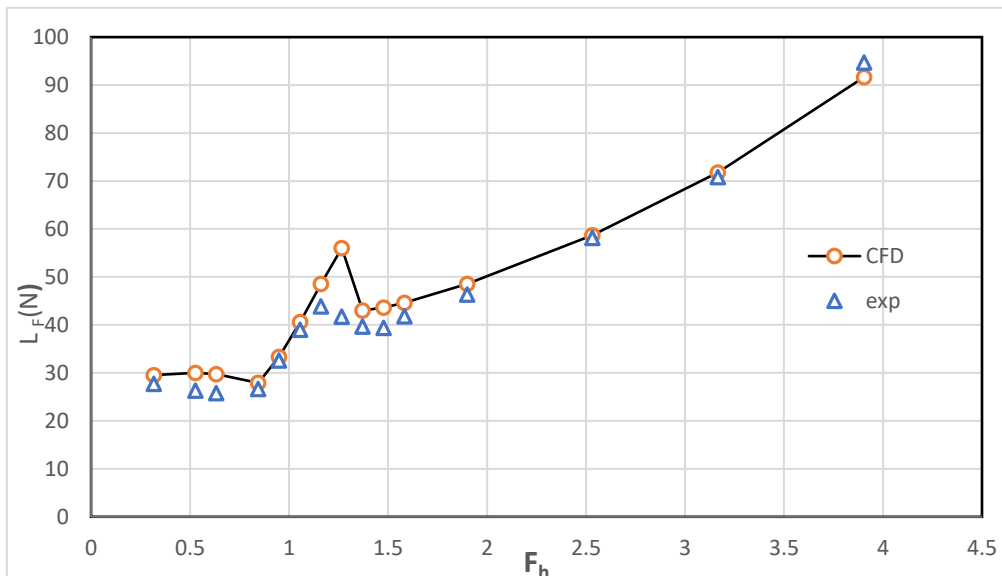

Figure 8 Experimental and numerical Lift force

5.1.5   Wave pattern

The numerical and experimental wave pattern is similar at speed 0.3m/s as shown in Figure 9. The free surface deformation at the displacement speed of 0.3m/s is not significant. In the low-speed region, there is no high deformation at the hull side, the wetted chine experimentally and numerically equal to 558.8mm and 620.9 mm sequentially. Also, there is partial ventilation at transom equals to 2.12 mm experimentally and 3.23 mm numerically
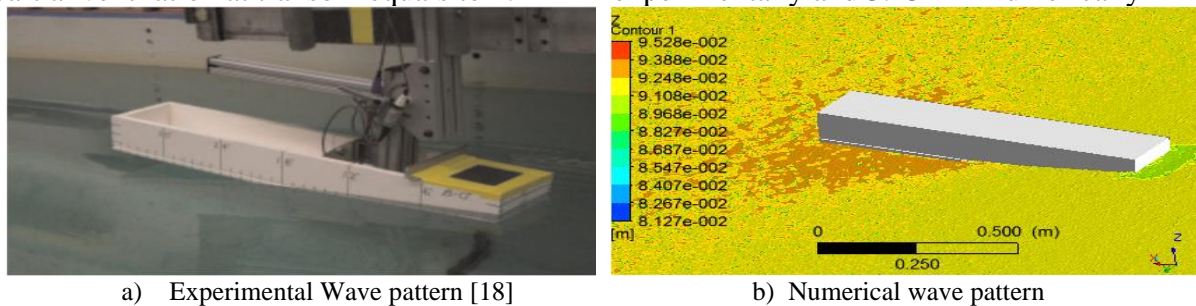

a)   Experimental Wave pattern [18]   b) Numerical wave pattern

Figure 9 Wave pattern comparison at speed of 0.3 m/s.

Figure 10 shows a similarity in the generated wave pattern numerically and experimentally at a speed of 1.8m/s. There is a high deformation on the free surface at the planing speed of 1.8m/s. While the waves about the hull side increase in height leading to an increase in wetted chine equal to 635.42 mm numerically and 609.6 mm experimentally, further the free surface drops at the transom. For the numerical and experimental generated wave pattern, high deformation occurs on the free surface and full ventilation at transom equal to 56.73 mm experimentally and 59.03 mm numerically.
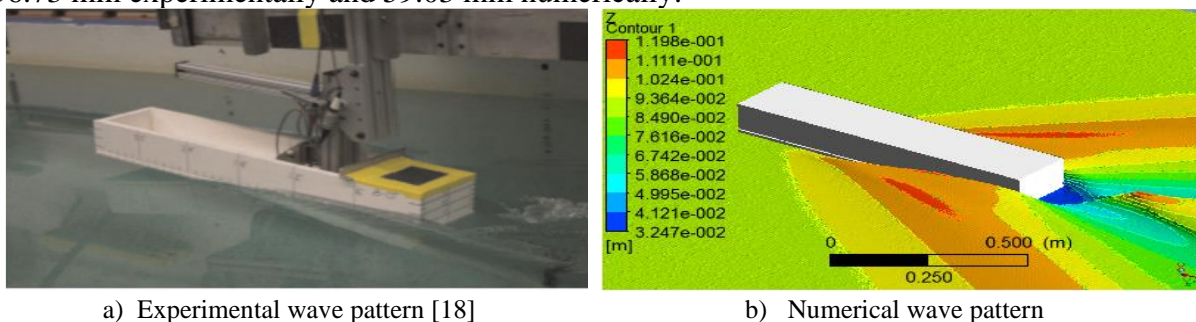

a) Experimental wave pattern [18]   b) Numerical wave pattern

Figure 10 Wave pattern comparison at speed 1.8 m/s

4.2 Solitary Wave Formation and Effects

In this section, the complex hydrodynamic phenomena of solitary wave or soliton formation will be discussed. The solitary wave requires a specific situation to occur such as a shallow channel waterway. When a hull is moving at critical speed in a shallow channel, the solitary wave will be observed. Table 4 shows the solitary waves establishment positions, and amplitudes for critical speeds which are 0.8, 0.9, 1, 1.1, 1.2 m/s. The amplitude of the solitary wave increases with the increase in wave speed. At speed 1.2m/s, the generated solitary wave is at amidships which has the highest amplitude of 0.05960 m. The solitary wave shifts forward till positioned at the front of the hull, which leads to fluid flow about the hull to be more complex.

Table 4: properties the solitary wave at a range of critical speed

Critical speed m/s	location of the wave formation numerically	Maximum wave amplitude (m)	location of the wave formation experimentally
0.60	No wave	-	No wave
0.80	3.3m ahead of model	0.0133	3 m ahead of model
0.90	1.2m ahead of model	0.0263	1 m ahead of model
1.00	0.3m ahead of model	0.035	at Bow
1.10	at Bow	0.0414	at Amidships
1.20	at Amidships	0.0596	supercritical swept 10-deg

The solitary wave establishes itself at different locations along the hull within the range of critical speeds and moves forward on the hull with time. Figure 11 shows the solitary wave formation steps. Firstly, the divergent waves hit the channel side at t= 2.4 seconds and increase the pressure on the channel sidewall. Secondly, the waves are reflected from the channel side and encounter other divergent waves generated from the hull after 4 seconds. Thirdly, the solitary wave becomes Perpendicular to the hull at t= 10 seconds. Afterwards, the wave shifts forward at t= 14.2 seconds until the maximum amplitude formulates at a position of 0.3m after the hull. The next pulse of the wave is produced at t= 18 seconds. As the hull moves in a shallow channel, it produces a pulse wave repeated every 23 seconds.
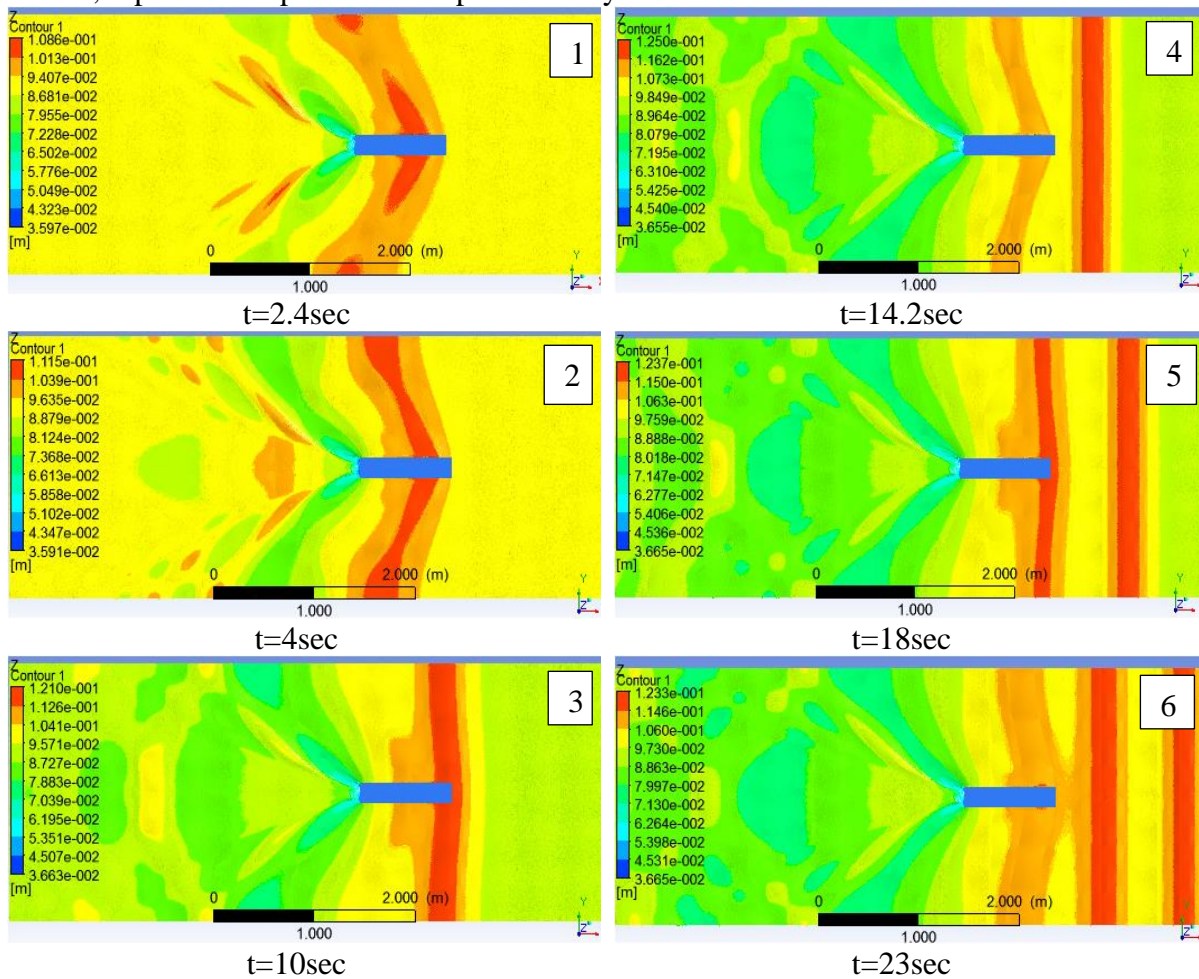

t=2.4sec

t=4sec

t=10sec

t=14.2sec

t=18sec

t=23sec

Figure 11 Solitary wave formulation steps at speed 1m/s

Figure 12 represents the change in a trim moment, lift force, and total resistance on the hull at the critical speed versus time. The maximum trim moment and maximum lift force occur on the hull at the same time. The effect of a solitary wave on the moment and lift force curves

144

Numerical prediction of solitary wave formation for
Planing hull in shallow water channels

Tamer M. Ahmed, Ahmed O. Elaghbash,
Adel A. Banawan, Yasser M. Ahmed, Amany M. Hassan.

is like a sinusoidal wave. The instantaneous values of the trim moment and lift force relate to the location of the solitary waveform and speed.
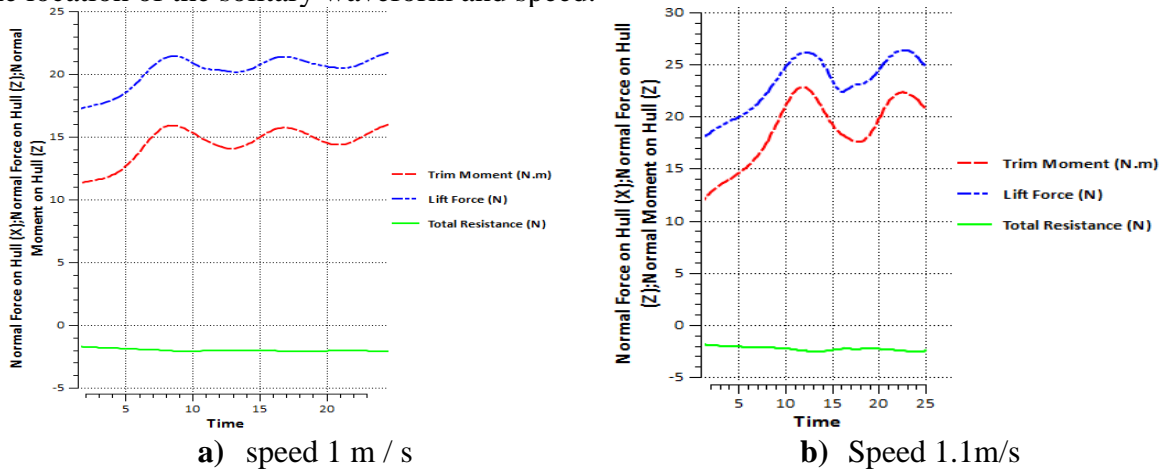

a) speed 1 m / s   **b)** Speed 1.1m/s

Figure 12 solitary wave effects on a trim moment, lift force, and total resistance

4.3 Comparison between hydrodynamic performance in Shallow Channel and Open Water

Figure 13 shows the difference between the shallow channel and deep water hydrodynamic pressure around the hull at a critical speed. Figure 13 (b) and (d) show an increased wetted surface area on the hull side and hull bottom in a shallow channel at critical speed compared with the wetted surface area in open water that is shown in Figure 13 (a) and (c). The maximum hydrodynamic pressure in Figure 13 (b) and (d) at hull piercing on the water. It's higher than that on the hull in Figure 13 (a) and (c). The pressure distributions around the hull at critical speed are unstable with time as a result of solitary waves formation.
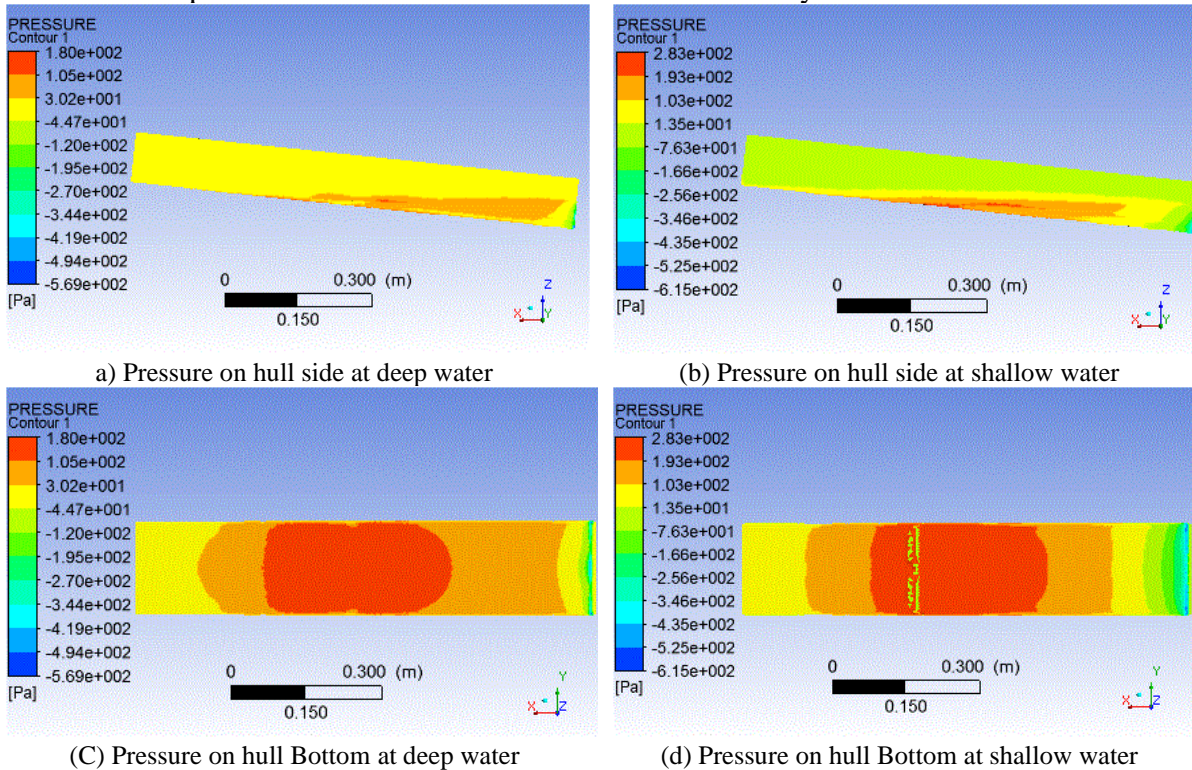

a) Pressure on hull side at deep water   (b) Pressure on hull side at shallow water

(C) Pressure on hull Bottom at deep water   (d) Pressure on hull Bottom at shallow water
Figure 13 Hydrodynamic pressure around the hull

Figure 14 a) and b) show the wave elevation comparison between open water and shallow water channel at speed (1m/s). The maximum wave height at the shallow water channel equals 0.069m. On the other hand, the maximum wave height at deep water equals 0.038m. The elevation of the wave in the shallow channel increases by about 81% from deep water. In

shallow channel (Figure 14b), the wave elevation increases and the solitary wave occurs at a critical speed surface which leads to an increase in the wave-making resistance compared with open water.
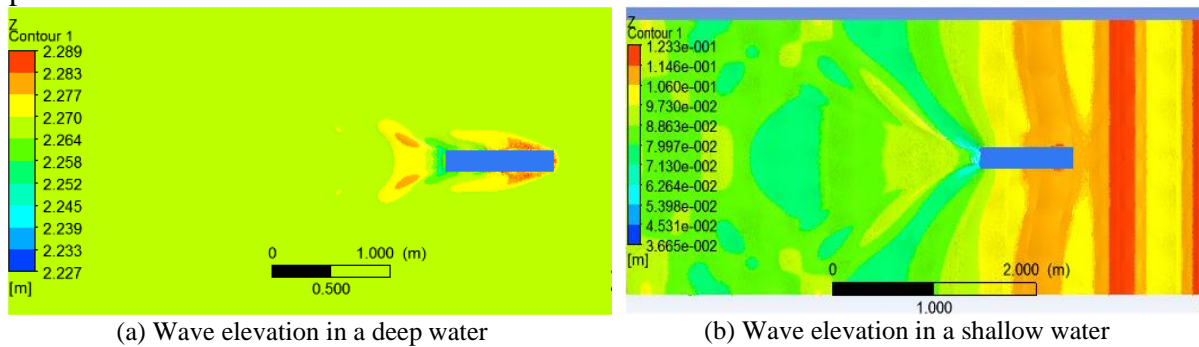

(a) Wave elevation in a deep water   (b) Wave elevation in a shallow water

Figure 14 wave systems comparison between a shallow channel and open water at speed 1m/s.
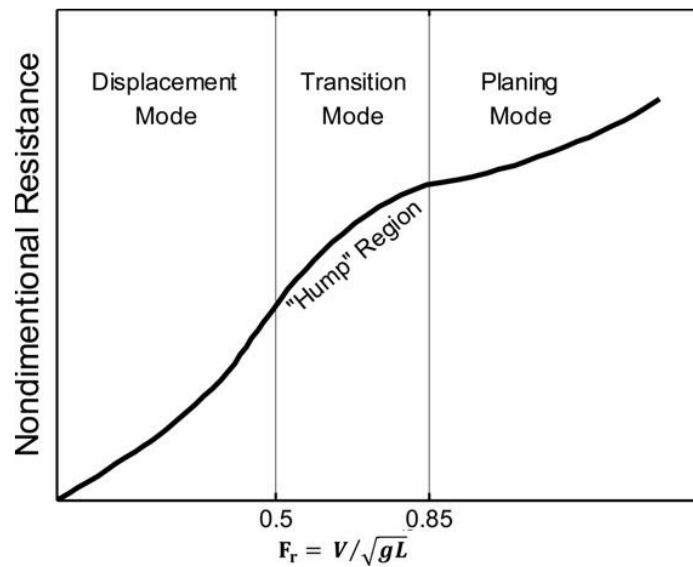

Figure 15 Total resistance of planing hull in deep water [19].

Figure 15 explains the total resistance in deep water for three regions of speed. When the Froude number is in the range of 0.5 this called displacement mode, and the total resistance increases with speed. For semi-displacement speed, the hump of resistance occurs at 0.5< Fr< 0.85 as a result of superposition in the wave system. After that, the total resistance increases with speed at the planing range Fr>0.85. This general figure for the total resistance of the planing hull in deep water is similar to deep water carve in Figure 16, which shows the total resistance in shallow water channels compared with the total resistance in deep water. The total resistance in deep water at the low speeds is not exactly similar to the total resistance in the shallow channel. Firstly, in the deep water, the chart increases gradually until the appearance of the hump which increases resistance as a result of a superposition between two crests or two troughs in the wave system. Also, there is a hollow that causes the total resistance to decrease because the crest cancels the trough in the wave system. Secondly, the total resistance in shallow water is rising rapidly in the critical speed period (0.8---1.2m/s). The maximum difference between total resistance in shallow water and total resistance in deep water is equal to 43% at speed 0.9m/s. The total resistance in the supercritical speed range increases dramatically with speed increase. Lastly, the total resistance in the shallow channel is much higher than the total resistance in open water.
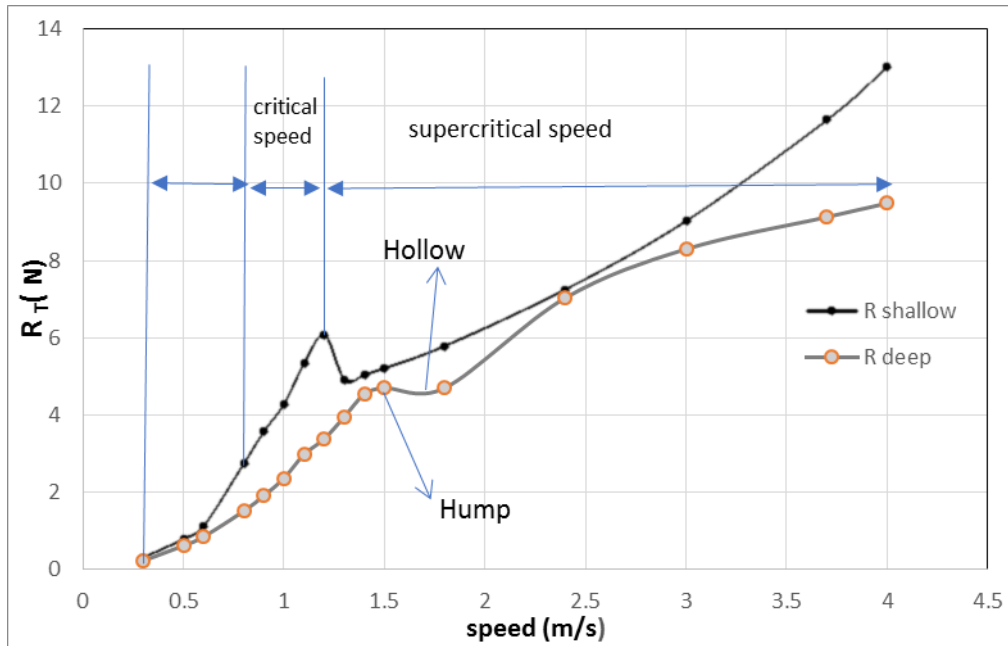
Numerical prediction of solitary wave formation for
Planing hull in shallow water channels

Tamer M. Ahmed, Ahmed O. Elaghbash,
Adel A. Banawan, Yasser M. Ahmed, Amany M. Hassan.

Figure 16 Comparison between the total resistance in shallow water channel and the total resistance in deep water

5. Conclusion

In this article, the RANS equations are solved by ANSYS-CFX code to simulate a small high-speed hull form moving in a shallow channel and open water. The total resistance and wave pattern of the planing hull model at three regions of speed (subcritical, critical, and supercritical) moving in the shallow channel have been numerically simulated.

In the shallow water channel, the total average error equals to 7% for numerical lift force, 8% for numerical total resistance compared with available experimental results. The numerical analysis well captured the wave pattern. The numerical results give good agreement over the whole range of speeds with the experimental results except at the maximum critical speed 1.2m/s which resulted in error equal to 34% for lift force and 26% for total resistance.

In the current study, the steps of the solitary wave formulation have been described at the critical speeds. The amplitudes of the solitary waves were determined at the critical speeds of 0.8, 0.9, 1, 1.1, and 1.2 m/s where the amplitudes were found equal to 0.0133, 0.0263, 0.035, 0.0414, and 0.0596m respectively.

The amplitude of the solitary wave increases whenever there is an increase in the critical speeds. Also, this investigation defined the locations of the solitary wave formulation. Solitary wave formulates in front of the hull at the lower range of critical speed. However, at the higher range of critical speed, it formulates on the hull.

The solitary wave formation increases the wetted surface area and the free surface deformation. Also, causes fluctuation in the trim moment, and lift force on the planing hull depends on the location and amplitude of the solitary wave. The total resistance on the hull in the shallow channel is higher than the total resistance in open water. The maximum difference is 43% which takes place at a critical speed 0.9m/s.

In conclusion, the worst effect on the planing hull in shallow channel occurs at critical speed range, where solitary wave formulates. So boat drivers must avoid sailing at critical speed range.

147

REFERENCES

[1]   A. Tafuni, I. Sahin, and M. Hyman, "Numerical investigation of wave elevation and bottom pressure generated by a planing hull in finite-depth water," *Appl. Ocean Res.*, vol. 58, pp. 281–291, 2016. https://doi.org/10.1016/j.apor.2016.04.002

[2]   V. Kerman, "The Impact on Seaplane Floats During Landing," Washington, No 321, 1929.

[3]   T. B.R, Savander, S.M, Scorpio, R.K, "Steady Hydrodynamic Analysis of Planing Surfaces," *J. Sh. Res.*, vol. 46, pp. 248–279, 2002.

[4]   S. D. S. Xue-Nong Chen, "A Slender Ship Moving at a Near-Critical Speed in a Shallow Channel," *J. Fluid Mech.*, vol. 291, no. May 1995, pp. 263–285, 1995. https://doi.org/10.1017/S0022112095002692

[5]   K. W. Christopher, "Effect of Shallow Water on the Hydrodynamic Characteristics of a Flat-Bottom Planing Surface." NACA, Washington, 1956.

[6]   C. J. Reyling, "An experimental study of planing surfaces operating in shallow water," new jersey, 1976.

[7]   A. Iafrati and R. Broglia, "Comparison between 2D+t potential flow models and 3d rans for planing hull hydrodynamics," *Ital. Sh. Model Basin*, no. December 2016, pp. 6–9, 1955.

[8]   F. Di Caterino, R. Niazmand Bilandi, S. Mancini, A. Dashtimanesh, and M. DE CARLINI, "A numerical way for a stepped planing hull design and optimization," *NAV Int. Conf. Sh. Shipp. Res.*, no. 221499, pp. 220–229, 2018.

[9]   R. N. Bilandi, S. Mancini, L. Vitiello, S. Miranda, and M. De Carlini, "A validation of symmetric 2D + T model based on single-stepped planing hull towing tank tests," *J. Mar. Sci. Eng.*, vol. 6, no. 4, 2018. https://doi.org/10.3390/jmse6040136

[10]   S. Brizzolara and F. Serra, "Accuracy of CFD codes in the prediction of planing surfaces hydrodynamic characteristics," *2nd Int. Conf. Mar. Res. Transp.*, pp. 147–158, 2007.

[11]   A. S. Amir H. Nikseresht, "Numerical investigation of shallow water resistance of a planing vessel," *Int. J. Civ. Struct. Eng.*, vol. 3, no. 1, pp. 164–168, 2016.

[12]   S. Mancini, F. De Luca, and A. Ramolini, "Towards CFD guidelines for planing hull simulations based on the Naples Systematic Series," *7th Int. Conf. Comput. Methods Mar. Eng. Mar. 2017*, vol. 2017–May, no. May, pp. 0–15, 2017.

[13]   Y. Wang, "Numerical Prediction of Resistance of Planning Vessel with RANS Method," *Int. Conf. Comput. Sci. Autom. Eng.*, no. Issue 2015, pp. 287–293, 2016. https://doi.org/10.2991/iccsae-15.2016.55

[14]   A. De Marco, S. Mancini, S. Miranda, R. Scognamiglio, and L. Vitiello, "Experimental and numerical hydrodynamic analysis of a stepped planing hull," *Appl. Ocean Res.*, vol. 64, pp. 135–154, 2017. https://doi.org/10.1016/j.apor.2017.02.004

[15]   M. Bakhtiari, S. Veysi, and H. Ghassemi, "Numerical Modeling of the Stepped Planing Hull in Calm Water," *Int. J. Eng.*, vol. 29, no. 2, 2016. https://doi.org/10.5829/idosi.ije.2016.29.02b.13

[16]   A. Dashtimanesh, A. Esfandiari, and S. Mancini, "Performance prediction of two-stepped planing hulls using morphing mesh approach," *J. Sh. Prod. Des.*, vol. 34, no. 3, pp. 236–248, 2018. https://doi.org/10.5957/JSPD.160046

[17]   F. Roshan, A. Dashtimanesh, and R. N. Bilandi, "Hydrodynamic characteristics of tunneled planing hull in calm water," *Brodogradnja*, vol. 71, no. 1, pp. 19–38, 2020. https://doi.org/10.21278/brod71102

[18]   M. G. Morabito, "Planing in Shallow Water at Critical Speed," *J. Sh. Res.*, vol. 57, no. 2, pp. 98–111, 2013. https://doi.org/10.5957/JOSR.57.2.120031

[19]   Marshall R, "All about Powerboats: Understanding design and performance," McGraw-Hill Professional, 2002.

Tamer M. Ahmed[1], tmahmed@alexu.edu.eg
Ahmed O. Elaghbash[1,2,] [*], eng-Ahmed.Elaghbah@alexu.edu.eg
                          men.aom90@gmail.com
Adel A. Banawan[1], adel.banawan@alexu.edu.eg
Yasser M. Ahmed[1], yasserahmed@alexu.edu.eg
Amany M. Hassan[1], amany.m.hassan@gmail.com

[1]Department of Naval Architecture and Marine Engineering, Faculty of Engineering, Alexandria University, Alexandria, Egypt.
[2]RSC for Marine Design and Research, Khartoum, Sudan.
*Corresponding author